Fiber bundle tracking method to analyze sheet molding compound microstructure based on computed tomography images

Ludwig Schöttl, Kay A. Weidenmann, Trevor Sabiston, Kaan Inal, Peter Elsner

Angaben zur Veröffentlichung / Publication details:

Schöttl, Ludwig, Kay A. Weidenmann, Trevor Sabiston, Kaan Inal, and Peter Elsner. 2021. "Fiber bundle tracking method to analyze sheet molding compound microstructure based on computed tomography images." *NDT & E International* 117: 102370. https://doi.org/10.1016/j.ndteint.2020.102370.

Fiber bundle tracking method to analyze sheet molding compound microstructure based on computed tomography images

Ludwig Schöttl [a,*], Kay André Weidenmann [a,b], Trevor Sabiston [c], Kaan Inal [c], Peter Elsner [a,d]

[a] Karlsruhe Institute of Technology, Institute for Applied Materials, Engelbert-Arnold-Straße 4, 76131, Karlsruhe, Germany
[b] University of Augsburg, Institute of Materials Resource Management, Werner-von-Siemens-Straße 6, 86159, Augsburg, Germany
[c] University of Waterloo, Department of Mechanical and Mechatronics Engineering, 295 Philip Street, N2L 3G1, Waterloo, Canada
[d] Fraunhofer Institute ICT, Joseph-von-Fraunhofer-Straße 7, 76327, Pfinztal, Germany

1. Introduction

1.1. Motivation

Discontinuous Fiber Reinforced Polymers (DicoFRP), such as Sheet Molding Compounds (SMC) are frequently applied in automotive mass production industry [1–3]. The way fibers are located and oriented on the microstructural level, significantly affects the mechanical properties of the macroscopic components. Consequently, it is essential to consider the microstructure in the design process.

Modern X-ray Micro-Computed Tomography (μCT) scans acquire two-dimensional projections of samples in a non-destructive way. By reconstructing the projections, a three-dimensional (3D) volumetric image is computed (e.g. Feldkamp et al. [4]). The microstructure is characterized by using image processing tools. In the contribution of Schladitz et al. [5], the authors introduced a method for determining the local fiber orientation, without identifying individual fibers based on an anisotropic Gaussian filter. Moreover, the fiber orientation data are associated with fatigue tests, in order to clarify the connection between microstructure and mechanical properties. In addition, Pinter et al. [6] compared different methods, which determine the local fiber orientation. It was figured out, that an approach based on the structure tensor, introduced by Krause et al. [7] works best in most cases [6]. One way to characterize the DicoFRP microstructure is to identify every individual fiber within the obtained volumetric image. An approach to characterize long fiber thermoplastic (LFT) microstructure is contributed by Pinter et al. [8]. In this contribution, tracking of every individual fiber was used to determine the fiber length distribution. Fibers were identified by using a circular voting filter and a skeletonization method. The approach was applied to a cylinder with ∅ 4 mm and 4 mm thickness of glass fiber

* Corresponding author.
E-mail address: ludwig.schoettl@kit.edu (L. Schöttl).

reinforced Polypropylene (PP). The reconstructed volumetric image resolution was 3 μm per voxel. By using transparent Polymethylmethacrylate (PMMA) matrix, Dumont et al. [9] in-plane optically observed the bundle microstructure of SMC before and after deformation. In-plane orientation, bending and width of manually selected fiber bundles were characterized. Another approach characterizing the fiber bundle microstructure is presented by Le et al. [10]. The authors Le et al. manually selected exemplary fiber bundle within µCT scans and measured the orientation, bending, thickness, width and cross section area. In both publications [9,10], the image voxel size is 7.5 μm

In addition to material science, image processing tools are frequently applied in medical science for the investigation of connections within the human brain. The authors Mori et al. [11,12] provide a technical review over magnetic resonance imaging based tracking methods. Tournier et al. [13] presented a second order probabilistic integration approach. The approach calculates the probability of each possible path and the most probable path corresponds to the expected curve. As a result, connections within the human brain were reliably tracked, even in regions where connections cross. Using Hessian matrix and eigenvalue analysis the authors Bhattacharya et al. [14] adapted the tracking methods by the authors Basser et al. [15] and Mori et al. [11,12] from the field of medical science in order to track the carbon fiber bundles of woven composites. Since the fiber bundles within woven composites are structured and orderly oriented, the authors Straumit et al. [16] segmented fiber bundles and matrix by using the structure tensor and determined a voxel-based representative volume element. The presented method in this contribution adapted the approach of Tournier et al. [13] to material science. As a result of the cone-beam µCT setup, the volumetric image resolution and the specimen size are directly coupled [17]. To identify individual fibers the image resolution has to be sufficiently smaller than the fiber diameter. The basic idea of the presented contribution is to use the fiber bundle arrangement of SMC, instead of the individual fibers for the microstructural characterization. By automatically tracking and clustering fiber bundles instead of individual fibers, the necessary image resolution increases and representative large specimen volumes are investigated.

1.2. Sheet molding compounds manufacturing

SMC is highly relevant for automotive mass production [1]. The microstructure of SMC, such as the fiber orientation is significantly affected by the manufacturing process. The semi-finished SMC manufacturing process is illustrated in Fig. 1. First, continuous fiber rovings are chopped into fiber bundles with defined length of typically 25.4 mm. The chopped fiber bundles drop randomly oriented onto a resin coated carrier foil and are then covered by another resin coated carrier foil. Going through the calendering zone, fiber bundles are infiltrated by resin. Subsequently, the semi-finished SMC rolls are stored for maturation. By using press molding technology, the semi-finished SMC is formed into the final geometry followed by curing of the matrix.

2. Fiber bundle tracking method

2.1. SMC microstructure classification

During the thermoforming process step, the chopped fiber bundles within the semi-finished SMC do not split up entirely into individually oriented fibers and are still arranged as bundles within the final component. Fig. 2 (a) shows the µCT cross section of a typical SMC microstructure and the fibers arranged in bundles.

In this contribution, the fiber bundles are classified on two different scale levels as follows.

Mesoscopic fiber bundles $\mathscr{R}$ emerge from the chopped fiber rovings of the manufacturing process and consist of a large number of individual fibers. The fibers within a mesoscopic bundle run parallel and are located close together. Exemplary mesoscopic bundles are colored in Fig. 2 (b). Mesoscopic bundles are inhomogeneous and sub-bundles are observed in Fig. 2 (a). The substructure of mesoscopic bundles is classified by **microscopic** bundle $\mathscr{S}$. The shape of exemplary microscopic bundle is illustrated in Fig. 2 (c). In summary, mesoscopic bundles correspond to the chopped fiber bundles and consists of several microscopic bundles.

2.2. Fiber orientation principals

The most general way to describe the fiber orientation, is given by the distribution function $\psi(\boldsymbol{p})$ [19], where $\psi(\boldsymbol{p})$ returns a proportion value of fibers aligned in $\boldsymbol{p}$ direction. In addition to the distribution function $\psi(\boldsymbol{n})$, the fiber orientation can be described by using orientation tensors [19,20]. For instance, the second order orientation tensor is given by

$$\boldsymbol{N} = \oint \boldsymbol{p} \otimes \boldsymbol{p} \psi(\boldsymbol{p}) \mathrm{d}\boldsymbol{p}. \tag{1}$$

In practice, the distribution function ψ is usually not available. But based on N discrete unit fiber vectors $\boldsymbol{n}_i$, an empirically formulation of the second order orientation tensor $\boldsymbol{N}$ is given by

$$\boldsymbol{N} = \frac{1}{N} \sum_{\gamma=1}^{N} \boldsymbol{n}_\gamma \otimes \boldsymbol{n}_\gamma. \tag{2}$$

The normalized eigenvectors $\boldsymbol{v}$ of $\boldsymbol{N}$ mark the principal direction of

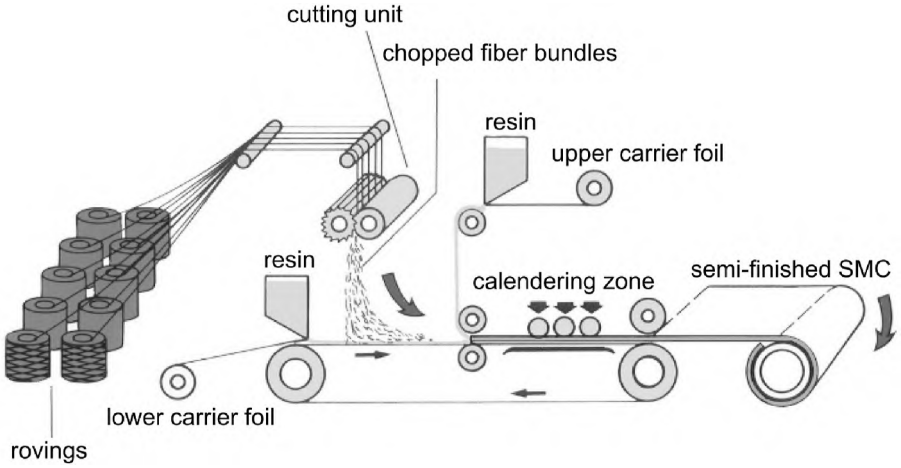

Fig. 1. Manufacturing process of semi-finished SMC [1,18].

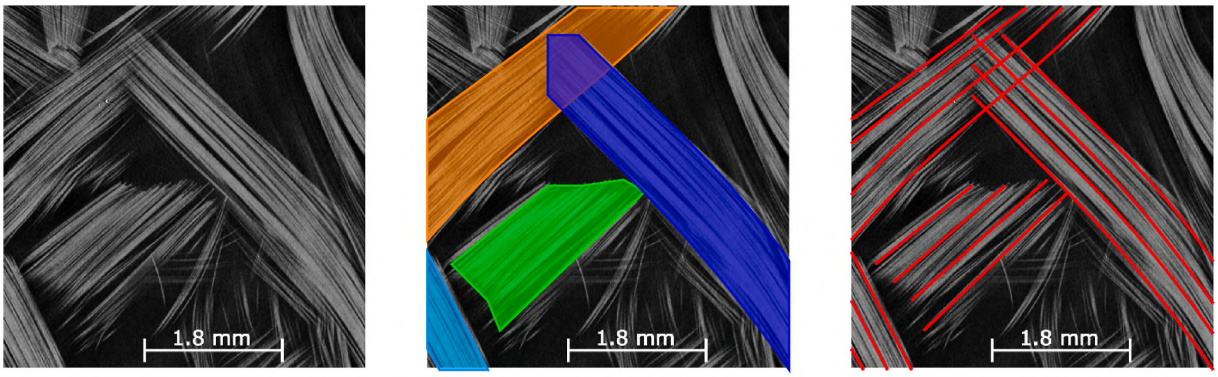

(a) SMC microstructure (b) Mesoscopic bundle $\mathcal{R}$ (c) Microscopic bundles $\mathcal{S}$

Fig. 2. μCT cross section of a SMC microstructure. Classification of the SMC microstructure by mesoscopic and microscopic bundles.

the fiber orientation distribution. The related eigenvalues λ represent the statistic proportion of fibers aligned in the according eigenvector direction [21]. All eigenvalues are sorted in the way that $\lambda_1 > \lambda_2 > \lambda_3$. Consequently, the eigenvector $\boldsymbol{v}_1$ represents the most relevant fiber orientation.

2.3. Probabilistic streamline tracking method

This contribution introduces an iterative, discrete integration method for tracking of microscopic bundles. By using the local fiber orientation data $\boldsymbol{n}(x,y,z)$, a trajectory is stepwise determined by moving along the highest probabilistic voxel path. Located at voxel $\boldsymbol{x}_i$, several potential next iteration step voxels $\tilde{\boldsymbol{x}}_j$ are identified by lower radius R_1, upper radius R_2 and aperture angle θ (cf. Fig. 3 (a)). The paths between $\boldsymbol{x}_i$ and the potential next iteration step voxels $\tilde{\boldsymbol{x}}_j$ is taking into account by quadratic space curves

$$\boldsymbol{s}_j(t) = \boldsymbol{s}_0 + \boldsymbol{s}_1 t + \boldsymbol{s}_2 t^2, \quad t = 0 \ldots 1, \tag{3}$$

defined by the conditions $\boldsymbol{s}_j(0) = \boldsymbol{x}_i$, $\boldsymbol{s}_j(1) = \tilde{\boldsymbol{x}}_j$ and $\boldsymbol{s}_j'(0) = \boldsymbol{n}_i$. The tangent of curve $\boldsymbol{s}_j(t)$ at $\tilde{\boldsymbol{x}}_j$ is given by $\boldsymbol{s}_j'(1)$. Define τ_j as the angle between the curve tangent $\boldsymbol{s}_j'(1)$ (blue) and the local fiber orientation $\tilde{\boldsymbol{n}}_j$ (red) of the potential next voxel in Fig. 3 (b).

$$\tau_j = \measuredangle\left(\tilde{\boldsymbol{n}}_j, \boldsymbol{s}'_j(1)\right) \tag{4}$$

Large τ pointing to a large deviation between curve $\boldsymbol{s}(t)$ and the fiber orientation data $\boldsymbol{n}$ and small τ indicating high accordance. Consequently, the voxel $\tilde{\boldsymbol{x}}_j$ with the smallest τ_j obtains the highest fiber orientation probability between trajectory and orientation data $\boldsymbol{n}$. As a result, the voxel $\tilde{\boldsymbol{x}}_j$ with the smallest τ_j becomes the next iteration step $\boldsymbol{x}_{i+1}$ (cf. Fig. 3 (c)). Iterating along the stepwise highest fiber orientation probability leads to a high global fiber orientation probability of the resulting trajectory.

Define $\mathcal{S}$ as the resulting trajectory, which contains all tracked iteration steps $\boldsymbol{x}_i$ and corresponding orientation vectors $\boldsymbol{n}_i$. In order to analyze the whole microstructure, a sufficient large number of trajectories $\mathcal{S}$ beginning at different starting points $\boldsymbol{x}_0$ are determined.

2.4. Clustering method

Several microscopic bundle trajectories $\mathcal{S}$ are acquired by the tracking method presented in Section 2.3. As introduced in Section 2.1, mesoscopic bundles consist of several microscopic bundles. By means of a clustering method, the trajectories related to the same mesoscopic bundle are merged together and as a result, the mesoscopic bundles are identified. The following two criteria are introduced to clarify, which

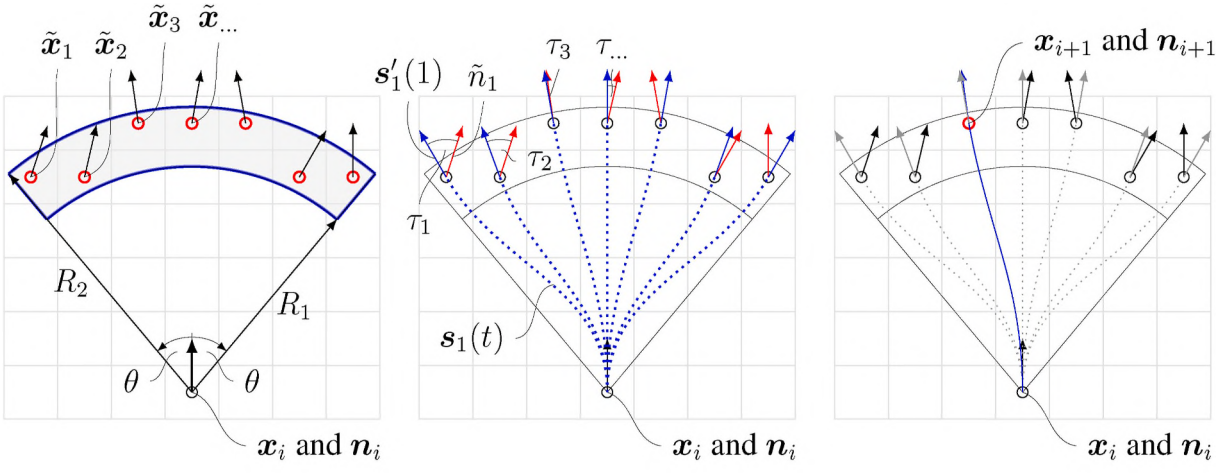

(a) Defining candidates $\tilde{\boldsymbol{x}}_j$ by using R_1, R_2 and θ (b) Defining curves $\boldsymbol{s}_j(t)$ and angles τ_j (c) Determining $\boldsymbol{x}_{i+1}$ and $\boldsymbol{n}_{i+1}$, related to smallest τ_j

Fig. 3. Illustrations of the schematic process of the probabilistic tracking approach.

microscopic bundle belong to the same mesoscopic bundle.

- **Distance:** Microscopic bundles within the same mesoscopic bundle are located close together and consequently, the distance between those microscopic bundles is small.
- **Orientation:** Microscopic bundles of the same mesoscopic bundle run parallel and consequently, the local orientation difference is small.

Appropriate factors for measuring these two criteria and taking them into account in clustering are presented below.

2.5. Distance measurement

Trajectory A is given by $\mathscr{S}_A = \{\boldsymbol{x}_i : i = 1 \ldots m_A\}$ and trajectory B by $\mathscr{S}_B = \{\boldsymbol{y}_j : j = 1 \ldots m_B\}$. Define $\tilde{\boldsymbol{y}}_i$ as the element of $\mathscr{S}_B$, with the smallest euclidean distance to $\boldsymbol{x}_i$. Conversely, define $\tilde{\boldsymbol{x}}_j \in \mathscr{S}_A$, with the smallest euclidean distance to $\boldsymbol{y}_j$ as shown in Fig. 4. The mean distance between trajectory $\mathscr{S}_A$ and $\mathscr{S}_B$ is given by

$$\widehat{d}_{AB} = \frac{1}{m_A}\sum_{i=1}^{mA} m_A \left|\boldsymbol{x}_i - \tilde{\boldsymbol{y}}_i\right| \quad \text{and} \quad \widehat{d}_{BA} = \frac{1}{m_B}\sum_{j=1}^{mB} m_B \left|\boldsymbol{y}_j - \tilde{\boldsymbol{x}}_j\right|. \tag{5}$$

Distance $\widehat{d}_{AB}$ (and $\widehat{d}_{BA}$) evaluates the average nearest distance from trajectory $\mathscr{S}_A$ to $\mathscr{S}_B$ (and reverse). However, in general $m_A \neq m_B$ and consequently, $\widehat{d}_{AB} \neq \widehat{d}_{BA}$. In order to define a commutative distance value, according to $d_{AB} = d_{BA}$, the distance between trajectory $\mathscr{S}_A$ and $\mathscr{S}_B$ is defined by $d_{AB} = \min(\widehat{d}_{AB}, \widehat{d}_{BA})$.

2.6. Orientation difference measurement

Additionally to the distance, also the orientation difference between two trajectories is considered for clustering. To compare the local orientation of two microscopic bundles, the trajectories are subdivided into sections of the same length. Calculating the second order orientation tensor $\boldsymbol{N}$ (cf. Equation (2)) of all sections by using the orientation vectors $\boldsymbol{n}_i$. The first eigenvector $\boldsymbol{v}_1$ of $\boldsymbol{N}$ shows the principle orientation of the corresponding section.

The orientation difference of two trajectories $\mathscr{S}_A$ and $\mathscr{S}_B$ is determined based on section pairs of both microscopic bundles. The first eigenvectors of the n_{AB}-number closest section pairs are compared. In this contribution, sections and section pairs are indicated by α. The first eigenvalues of the section pair α are labeled by $\boldsymbol{v}_\alpha$ and $\tilde{\boldsymbol{v}}_\alpha$. The orientation difference of the section pairs α is determined by the angle $\varphi_\alpha = \measuredangle(\tilde{\boldsymbol{v}}_\alpha, \boldsymbol{v}_\alpha)$ (cf. Fig. 5).

The overall orientation difference between two microscopic bundles $\mathscr{S}_A$ and $\mathscr{S}_B$ is described by the averaged angle over all n_{AB} closest section pairs

$$\varphi_{AB} = \frac{1}{n_{AB}}\sum_{\alpha=1}^{n_{AB}} \varphi_\alpha. \tag{6}$$

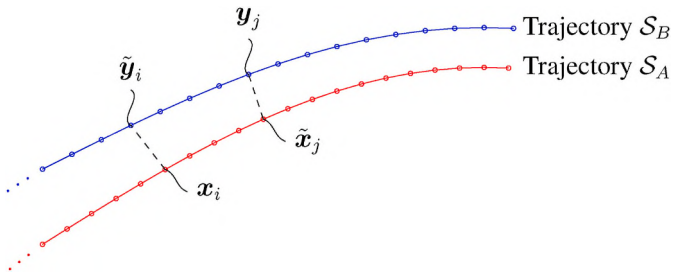

Fig. 4. The distance between the two trajectories $\mathscr{S}_A$ and $\mathscr{S}_B$.

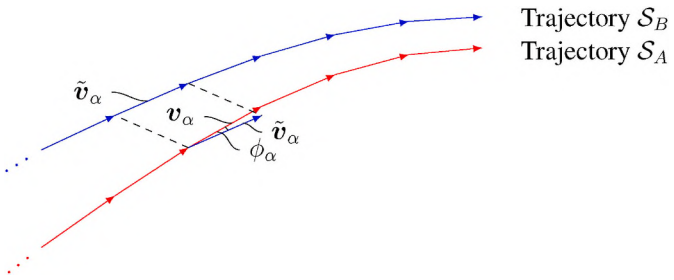

Fig. 5. The orientation difference φ_α of section pair α.

2.7. Hierarchical agglomerative clustering

Mesoscopic bundles are identified by clustering microscopic bundles. Stepwise close and parallel trajectories are merged to the same cluster. Two clusters $\mathscr{R}_A$ and $\mathscr{R}_B$ are compared by the averaged $\overline{d}_{AB}$ and $\overline{\varphi}_{AB}$ value, of all microscopic bundle pairs between both clusters. By taking the average distance $\overline{d}_{AB}$ and orientation difference $\overline{\varphi}_{AB}$ into account, the similarity value

$$\rho_{AB} = \frac{1}{\lambda_G + \lambda_O}\left(\lambda_O\left(\frac{k_O - \overline{\varphi}_{AB}}{k_O}\right) + \lambda_G\left(\frac{k_G - \overline{d}_{AB}}{k_G}\right)\right) \tag{7}$$

between cluster $\mathscr{R}_A$ and $\mathscr{R}_B$ is introduced. The average distance $\overline{d}_{AB}$ and the orientation difference $\overline{\varphi}_{AB}$ are normalized by k_G and k_O. Adapting the weighting factors λ_G and λ_O, the distance and orientation criteria impact is adjusted. The similarity value ρ_{AB} ranges from 0 to 1 and specifies the similarity of two clusters. In case of $\rho_{AB} = 1$, both clusters $\mathscr{R}_A$ and $\mathscr{R}_B$ are identical.

In this contribution, microscopic bundles are clustered by a state-of-the-art hierarchical agglomerative (bottom - up) clustering approach [22,23]. Initially all trajectories $\mathscr{S}$ form an individual cluster $\mathscr{R}_i = \{\mathscr{S}_i\}$, so that there are as many clusters as trajectories. The similarity value ρ_{AB} of all cluster pairs is determined in each clustering step. The cluster pair with the highest similarity is then merged together. As a result, the number of clusters is reduced by one in each iteration step. The clustering process is stopped, if the highest similarity drops below a defined threshold k_ρ, or if the difference of the highest similarity between two consecutive iteration steps is below a defined threshold Δk_ρ.

The hierarchical agglomerative clustering process is schematically illustrated in Fig. 6. Initially each trajectory $\mathscr{S}_{A\ldots H}$ forms an individual cluster $\mathscr{R}_{A\ldots H}$. In this example, the mesoscopic bundles are given by the final resulting microscopic bundle clusters $\mathscr{R}_{AB} = \{\mathscr{S}_A, \mathscr{S}_B\}$, $\mathscr{R}_{CDE} = \{\mathscr{S}_C, \mathscr{S}_D, \mathscr{S}_E\}$ and $\mathscr{R}_{FGH} = \{\mathscr{S}_F, \mathscr{S}_G, \mathscr{S}_H\}$ (cf. ellipses in Fig. 6).

3. Experimental

3.1. Image acquisition

A YXLON-CT precision µCT system with a flat panel PerkinElmer Y.

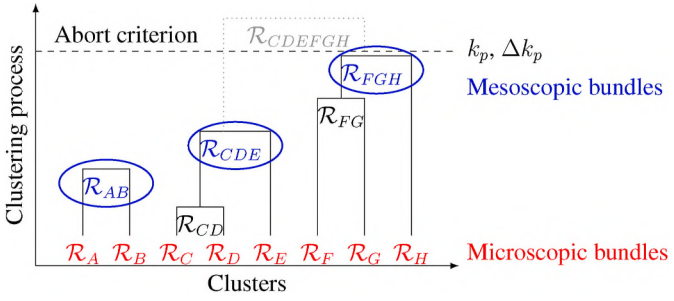

Fig. 6. Hierarchical agglomerative clustering.

XRD1620 detector with 2048 × 2048 pixels is used. The parameters of the performed µCT scans are listed in Table 1. The resulting volumetric images are reconstructed by applying the Feldkamp cone-beam algorithm [4].

3.2. Material

The investigate SMC sample is based on Unsaturated Polyester Polyurethane Hybrid (UPPH) resin system without fillers by Aliancys and is reinforced by discontinuous glass fibers from John Manville (GF Multistar 272). The fiber diameter is approximately 13.5μm, the chopped fiber bundle length 25.4mm and the nominal batch fiber content 41$wt.\%$. The semi-finished SMC is formed into plates of 800$mm\times$ 250$mm \times$ 3mm by press molding and samples are extracted by water jet.

3.3. Tracking and clustering parameter

Fig. 7 shows an overview of the applied tracking and clustering process. After performing the µCT scan and reconstructing the volumetric image, the fiber bundles and matrix are separated by using the momentum threshold introduced by Tsai [24]. Subsequently, the local fiber orientations $\boldsymbol{n}$ are determined by using the structure tensor (cf [7]), provided by the authors Pinter et al. [6]. The starting points $\boldsymbol{x}_0$ of the fiber bundle tracking process are defined based on an equidistant rectangular grid. The parameter R_1, R_2 and θ are selected to 0.06 mm, 0.27 mm and 5°, respectively. Subsequently after tracking the microscopic bundles $\mathscr{S}$, the clustering method is applied. The normalization values k_O is selected to 90° and k_G to the length of the longest trajectory. Calculating the similarity value ρ, the distance criterion $\overline{d}$ is weighted double-times ($\lambda_G = 2$), compared to the orientation criterion $\overline{\varphi}$ ($\lambda_O = 1$). The clustering iteration ends after the highest similarity dropped below $k_p = 0.97$.

4. Results

For validating the introduced methods, the µCT volumetric image, intermediate and final results are presented in Fig. 8. Fig. 8 (a) illustrates a representative µCT cross section of the analyzed SMC microstructure. The starting points $\boldsymbol{x}_0$ of the fiber bundle tracking process are illustrated by red points in Fig. 8 (b). All starting points $\boldsymbol{x}_0$ are located within the representative µCT cross section. The microscopic bundles are three-dimensionally tracked within the whole volumetric image by using the introduced methods and the parameters in Section 3.3. All determined trajectories $\mathscr{S}$, with a length of more than 0.81 mm are plotted in Fig. 8 (c). The fiber bundle-matrix separated microstructure is imaged binary in the background (fiber bundles in white and matrix in black). The trajectory colors are randomly selected. Applying the presented clustering method, the microscopic bundle trajectories $\mathscr{S}$ are assigned to clusters of the same mesoscopic bundle $\mathscr{R}$. Fig. 8 (d) illustrates the clustered mesoscopic bundles by uniform colors, which contain at least 5 microscopic bundles.

In addition to the results in Fig. 8, the introduced method is applied to two large-scale SMC microstructure volumes. Fig. 9 (a) and Fig. 10 (a) show the volumetric images of the analyzed SMC microstructures. Both microstructures are also investigated by the introduced methods and the parameters in Section 3.3. The clustered fiber bundles are visualized three-dimensionally in Fig. 9 (b) and Fig. 10 (b). Furthermore, Fig. 10 (c) shows the clustered fiber bundles more detailed within an enlarged regions (black box).

Table 1
Parameters of the performed µCT scans.

Parameter	Scan no. 1	Scan no. 2
X-ray tube head	Transmission	Reflection
No. of projections	2400	1950
Acceleration voltage	130 kV	150 kV
Current	0.03 mA	0.2 mA
Exposure/Integration time	1000 ms	500 ms
Frame binning	2	2
Voxel size	9.05 μm	6.80 μm

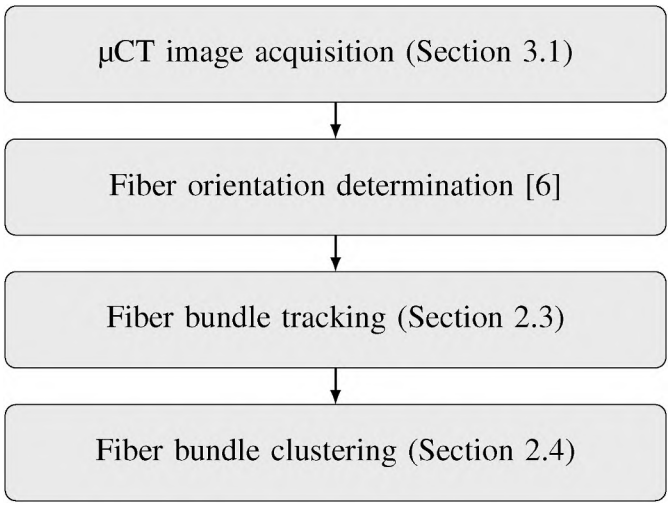

Fig. 7. Overview of the introduced approach for tracking and clustering of SMC fiber bundle.

5. Discussion

There are several state-of-the-art image processing tools for the analysis of fiber reinforced polymer microstructures within volumetric images [5–8]. The introduced tracking method adapts the approach of Tournier et al. [13] by iterative moving along the stepwise highest probabilistic path. The tracking method is applied to the SMC microstructure shown in Fig. 8 (a). The starting points of the fiber bundle tracking process are plotted in Fig. 8 (b) and the tracked microscopic bundles trajectories in Fig. 8 (c). The background in Fig. 8 (b)–(c) illustrates the representative µCT cross section of the analyzed SMC microstructure. The tracked microscopic bundles correspond to the fiber bundles within the µCT cross section (background). Fiber bundles above or below of the µCT cross section are not visible within it. The microscopic bundles are tracked in 3D and consequently, fiber bundles are identified which are not completely visible within the µCT cross section (cf. dotted ellipse No. 1 in Fig. 8 (c))

Based on the introduced distance and orientation criteria the clustering method identifies and merges microscopic bundles which belong to the same mesoscopic bundle. The clustered fiber bundles are visualized by uniform colors in Fig. 8 (d). The individual mesoscopic bundles correspond to the fiber bundles within the µCT cross section (background). However, crossing mesoscopic bundles with similar orientation are difficult to separate. For instance in Fig. 8 (d), the orange and yellow fiber bundle are not clustered together, due to the crossing blue colored fiber bundle (cf. dotted ellipse No. 2). Furthermore, some fiber bundles are slightly separated during press molding (cf. dotted ellipse No. 3). It is difficult to evaluate, if these fiber bundles are considered as one or two mesoscopic bundles. In addition to the results in Fig. 8, the introduced methods are applied to two large-scale SMC microstructures. The volumetric image of the two SMC specimens is shown in Fig. 9 (a) and Fig. 10 (a). Fig. 9 (b) and Fig. 10 (b) illustrate the tracked and clustered SMC fiber bundles in 3D. An enlarged illustration of Fig. 10 (b) is shown in Fig. 10 (c). In the contribution of Dumont et al. [9] and Le et al. [10], the authors manually selected fiber bundles within images. For instance, in the contribution of Dumont et al. [9] 108 fiber bundles are used to characterize the global orientation. In contrast, the introduced method in this paper automatically determines microscopic and mesoscopic

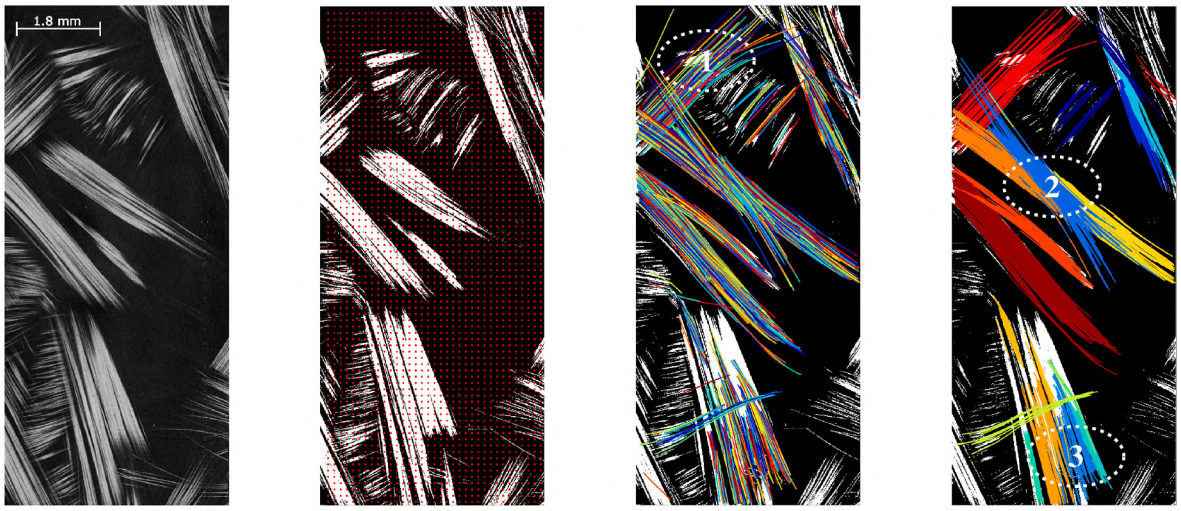

Fig. 8. Applying the presented methods to an SMC microstructure. The voxel size of the volumetric image (scan no. 1) is 9.05 μm.

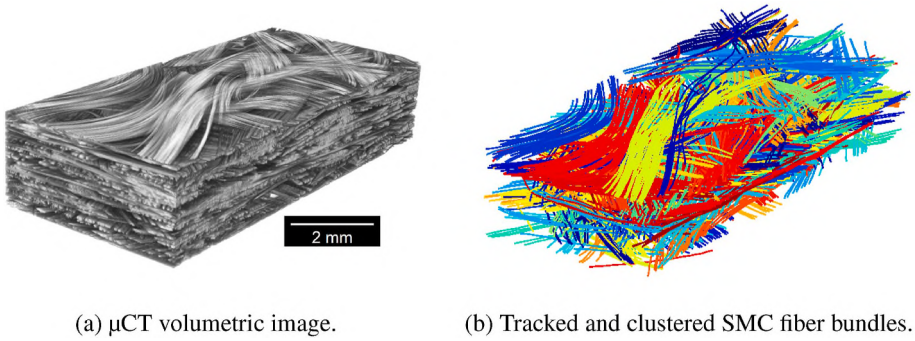

Fig. 9. 3D visualization of the tracked and clustered SMC fiber bundles. Height, length and thickness of the analyzed microstructure is 2.95 mm, 10.81 mm and 4.86 mm, respectively. The voxel size of the volumetric image (scan no. 1) is 9.05 μm. Only clustered fiber bundles with a minimum of 100 sub-bundles are visualized.

fiber bundles in a reproducible way. This offers the opportunity to analyze a large number of fiber bundles and take them into account for the microstructure characterization. In the contribution of Pinter et al. [8], the authors track individual fibers based on volumetric images with voxel size of 3 μm. Due to the high image resolution that is required for tracking individual fibers, the overall measured sample size is limited. Applying the introduced methods and tracking fiber bundles instead of individual fibers, the necessary voxel size increases up to 9.05 μm

Besides SMC, fibers are arranged as bundles within in woven composites. In contrast to SMC, in woven composites the fiber bundles are structured and not randomly oriented. The authors Bhattacharya et al. [14] and Straumit et al. [16] track the carbon fiber bundles within woven composites. In both publications [14,16], the authors make use of the fact that the fiber bundles in woven fabrics are arranged in a structured and periodical manner. Furthermore, due to the structured and periodic microstructure, the number of fiber bundles within a specific unit cell can be clearly calculated and used as input parameter for the clustering process [16]. In this contribution, SMC fiber bundles are tracked by a similar method of those introduced by Mori et al. [11,12] and applied by Bhattacharya et al. [14]. However, SMC fiber bundles are randomly oriented and not structured. Consequently, the clustering of SMC fiber bundles is much more complex compared to woven composites because the number of fiber bundles per volume is not clear and the fiber bundles are randomly oriented. The decisive advantage of the presented methods compared to the other publications [14,16] is the ability to handle fiber bundles in unstructured and randomly oriented SMC microstructures.

6. Conclusion

This contribution deals with microstructure characterization methods for Sheet Molding Compounds (SMC) by means of Micro-Computed Tomography (µCT) scanning. Methods for the automatically tracking and clustering of SMC fiber bundles based on volumetric images and fiber orientation data are introduced. The methods enable to characterize the microstructure of SMC based on the fiber bundles instead of individual fibers. Consequently, the necessary µCT resolution is increased and larger microstructure volumes can be analyzed.

The introduced approach consists of two parts. First, a probabilistic streamline method tracks microscopic bundles by means of fiber orientation data. The presented tracking method iteratively determines the stepwise highest probabilistic path along the microscopic bundles that meet the challenge of other crossing fiber bundles. Mesoscopic fiber bundles that emerge from the chopped fiber roving within the semi-finished SMC manufacturing process and consist of several parallel and closely aligned fibers. Criteria are introduced to quantify the difference in distance and orientation between microscopic bundles. Based on the presented distance and orientation criteria, the mesoscopic bundles are identified by using an agglomerating hierarchical clustering algorithm. The key advantage of the presented methods is the ability to identify fiber bundles in unstructured and randomly oriented SMC microstructures. For validation, the fiber bundle within a representative

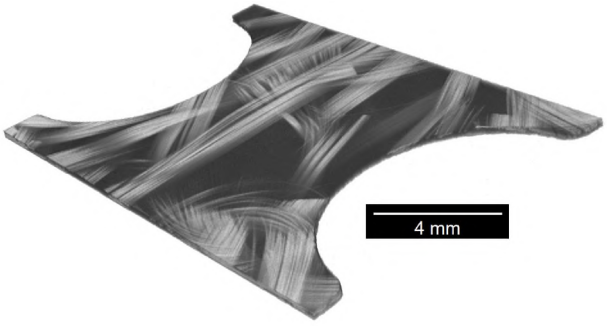

(a) µCT volumetric image.

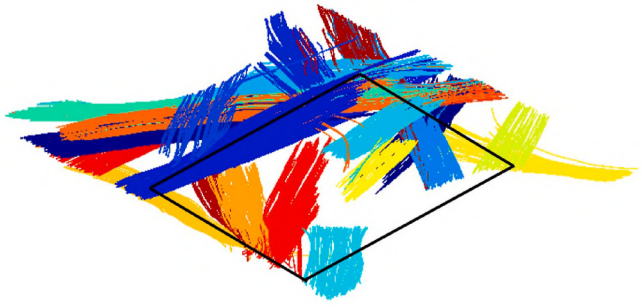

(b) Tracked and clustered SMC fiber bundles.

(c) Tracked and clustered SMC fiber bundles within the enlarged region.

Fig. 10. The tracked and clustered SMC fiber bundles within the notch region of a SMC tensile specimen. Figure (a) visualizes the µCT image, (b) the resulting fiber bundles and (c) the resulting fiber bundles within the enlarged black box more detailed. Voxel size of the volumetric image (scan no. 2) is 6.80 μm. Only clustered fiber bundles with a minimum of 50 sub-bundles are visualized.

SMC microstructure are tracked and clustered by using the presented methods. The results correspond to the µCT cross section of the analyzed SMC microstructure. Finally, the applicability of the presented methods is demonstrated on two large-scale 3D SMC microstructures.

Nomenclature

$\mathscr{R}$	Mesoscopic bundles and clusters
$\mathscr{S}$	Microscopic bundles and trajecories
$\boldsymbol{N}$	Second order orientation tensor
$\boldsymbol{n}$	Orientation vector
$\boldsymbol{v}$	(First) Eigenvector of $\boldsymbol{N}$
$\boldsymbol{x}$	Voxel and tracking point position vector
λ_O/λ_G	Weighting factors
ρ	Similarity value
τ, φ	Difference angle
θ	Aperture angle
$\widetilde{(\cdot)}$	Closest voxel/section
d	Euclidean distance

CRediT authorship contribution statement

Ludwig Schöttl: Conceptualization, Methodology, Software, Validation, Formal analysis, Investigation, Data curation, Writing - original draft, Visualization, Project administration. **Kay André Weidenmann:** Conceptualization, Resources, Writing - review & editing, Supervision, Funding acquisition. **Trevor Sabiston:** Conceptualization, Writing - review & editing. **Kaan Inal:** Conceptualization, Writing - review & editing, Supervision. **Peter Elsner:** Conceptualization, Resources, Writing - review & editing, Supervision, Funding acquisition.

Declaration of competing interest

The authors declare that they have no known competing financial interests or personal relationships that could have appeared to influence the work reported in this paper.

Acknowledgments

The research documented in this manuscript has been funded by the German Research Foundation (DFG) within the International Research Training Group “Integrated engineering of continuous-discontinuous long fiber reinforced polymer structures” (GRK 2078). The support by the German Research Foundation (DFG) is gratefully acknowledged. As well the authors grateful appreciate the support of Fraunhofer ICT by supplying the experimental forming results of the samples, which were finished under the project leadership of Sergej Ilinzeer. Moreover, the authors greatful appreciate Pascal Pinter for providing his fiber orientation method.

k_O/k_G Normalization parameters
R_1/R_2 Minimum/Maximum search radius

Appendix A. Supplementary data

Supplementary data to this article can be found online at https://doi.org/10.1016/j.ndteint.2020.102370.

Authors contribution

Ludwig Schöttl developed, implemented and applied the methods presented in this paper. He also wrote the first draft of the paper. The image processing tool for determining the local fiber orientation on the voxel level based on volumetric gray value images was contributed by Pascal Pinter. The work was initiated and initialized by Ludwig Schöttl and Kaan Inal during the research stay of Ludwig Schöttl at the University of Waterloo. Kay André Weidenmann and Peter Elsner supervised and coordinated the implementation and application by Ludwig Schöttl at the Karlsruhe Institute of Technology. Kay André Weidenmann, Trevor Sabiston, Kaan Inal and Peter Elsner thoroughly revised the paper.

References

[1] Eyerer P, Hirth T, Elsner P. Polymer engineering. Springer; 2008.
[2] Jones RM. Mechanics of composite materials. Taylor & Francis; 1999.
[3] Talreja R, Singh CV. Damage and failure of composite materials. Cambridge University Press; 2012.
[4] Feldkamp LA, Davis LC, Kress JW. Practical cone-beam algorithm. J Opt Soc Am 1984;1(6):612–9.
[5] Schladitz K, Bueter A, Godehardt M, Wirjadi O, Fleckenstein J, Gerster T, Hassler U, Jaschek K, Maisl M, Maisl U, Mohr S, Netzelmann U, Potyra T, Steinhauser MO. Non-destructive characterization of fiber orientation in reinforced SMC as input for simulation based design. Compos Struct 2017;160:195–203.
[6] Pinter P, Dietrich S, Bertram B, Kehrer L, Elsner P, Weidenmann KA. Comparison and error estimation of 3D fibre orientation analysis of computed tomography image data for fibre reinforced composites. NDT E Int 2018;95(26 – 35).
[7] Krause M, Hausherr JM, Burgeth B, Herrmann C, Krenkel W. Determination of the fibre orientation in composites using the structure tensor and local X-ray transform. J Mater Sci 2009;45(4):888–96.
[8] Pinter P, Bertram B, Weidenmann KA. A novel method for the determination of fibre length distributions from µCT-data. In: 6th conference on industrial computed Tomography; 2016.
[9] Dumont P, Vassaland JP, Orgéas L, Michaud V, Favier D, Manson JAE. Processing, characterisation and rheology of transparent concentrated fibre-bundle suspensions. Rheol Acta 2007;46(5):639–51.
[10] Le TH, Dumont PJJ, Orgéas L, Favier D, Salvo L, Boller E. X-ray phase contrast microtomography for the analysis of the fibrous microstructure of SMC composites. Compos Appl Sci Manuf 2008;39(1):91–103.
[11] Mori S, Crain BJ, Chacko VP, Van Zijl PCM. Three-dimensional tracking of axonal projections in the brain by magnetic resonance imaging. Ann Neurol 1999;45(2):265–9.
[12] Mori S, van Zijl PCM. Fiber tracking: principles and strategies – a technical review. NMR Biomed 2002;15:468–80.
[13] Tournier J-D, Calamante F, Connelly A. Improved probabilistic streamlines tractography by 2nd order integration over fibre orientation distributions. Proc. International Society for Magnetic Resonance in Medicine 2010;18.
[14] Bhattacharya A, Heinzl C, Amirkhanov A, Kastner J, Wenger R. MetaTracts - a method for robust extraction and visualization of carbon fiber bundles in fiber reinforced composites. IEEE pacific visualization symposium (PacificVis). 2015. p. 191–8. 2015.
[15] Basser PJ, Pajevic S, Pierpaoli C, Duda J, Aldroubi A. In vivo fiber tractography using DT-MRI data. Magn Reson Med 2000;44(4):625–32.
[16] Straumit I, Lomov SV, Wevers M. Quantification of the internal structure and automatic generation of voxel models of textile composites from X-ray computed tomography data. Compos Appl Sci Manuf 2015;69:150–8.
[17] Buzug TM. Computed Tomography. Springer; 2010.
[18] TechCenter Bayer. The Illustrations may no longer correspond to the currently used procedures or the current product portfolio of Bayer Group. www.plastics.bayer.com; 2008.
[19] Advani SG, Tucker CL. The use of tensors to describe and predict fiber orientation in short fiber composites. J Rheol 1987;31(8):751–84.
[20] Ken-Ichi K. Distribution of directional data and fabric tensor. Int J Eng Sci 1984;22(2):149–64.
[21] Nabiatek J. Modeling of fiber orientation during injection molding process of polymer composites. Polish Society of Composite Materials 2011;11(4):347–51.
[22] Ding C, He X. Cluster merging and splitting in hierarchical clustering algorithms. In: IEEE international conference on data mining, *2002*. Proceedings; 2002. p. 139–46. 2002.
[23] Wierzchon ST, Klopotek MA. Modern algorithms of cluster Analysis. Springer; 2018.
[24] Tsai W-H. Moment-preserving thresholding: a new approach. Comput Vis Graph Image Process 1985;29:377–93.